TÜBİTAK

Turkish Journal of Electrical Engineering & Computer Sciences

http://journals.tubitak.gov.tr/elektrik/

Research Article

Turk J Elec Eng & Comp Sci
(2017) 25: 2547 – 2553

doi:10.3906/elk-1605-86

Design and implementation of a six-port junction based on substrate integrated waveguide

Masoud JAFARI*, Gholamreza MORADI, Reza SARRAF SHIRAZI, Rashid MIRZAVAND

Department of Electrical Engineering, Amirkabir University of Technology, Tehran, Iran

Received: 08.05.2016 • **Accepted/Published Online:** 20.09.2016 • **Final Version:** 29.05.2017

Abstract: A six-port junction based on substrate integrated waveguide technology with high reliability and efficient performance is proposed in a sub-K-band of 21–23.5 GHz. This substrate integrated waveguide (SIW) six-port junction is constructed from three directional couplers and one T-junction power divider as fundamental components in SIW form, where using appropriate via techniques led to –6 dB coupling coefficients and –15 dB return loss. There is good agreement between the simulation and the measurement results.

Key words: Six-port, substrate integrated waveguide

1. Introduction

Six-port junctions have various applications in microwave engineering. They can be utilized in measuring the reflection coefficient of an unknown load. For this purpose, one of the six ports is considered as an incident port and another is connected to a load. By detecting the power that appears on the remaining four ports and tracing the q-circles, the reflection coefficient is obtained. It can also be applied to direct conversion receivers, where two input-isolated ports act as local oscillator (LO) and radio frequency (RF) inputs and the remaining four ports are the output I/Q signals of quadrature phase shift keying (QPSK) demodulation. In this case, the optimum state occurs when the phase differences of the q-circles are 90° and their amplitudes are equal. Additionally, they have many other applications, e.g., displacement detection, vibration measurement, mechanical stress diagnosis, and automotive radar calibration.

On the other hand, substrate integrated waveguides (SIWs) have high-power applications, especially in millimeter wave ranges. These waveguides are the planar versions of conventional rectangular waveguides, which are composed of two rows of metallic vias with predetermined diameter and distance period limited in top and bottom metallic layers. Many empirical formulas have been presented for the equivalent rectangular waveguide width of SIWs. In [1], the calculation of the propagation constant in SIW transmission lines, based on the concept of surface impedance with the method of moments (MOM), was performed. An empirical formula based on the calculation of eigenvalues of the admittance matrix was obtained with the least square approach [2]. A more accurate formulation was presented for special conditions and various dimension ratios by considering small error effects due to increasing period of vias [3]. Additionally, an empirical equation for the equivalent width of SIW, based on the method of lines, was proposed [4]. In this paper, a SIW six-port junction

*Correspondence: masoud1986@aut.ac.ir

is implemented in the K-band using empirical Eq. (1) for determining the equivalent width of the SIW [5]:

$$w_{eff} = w - \frac{d^2}{0.95s}, \tag{1}$$

where w is the distance of the center of two rows of the via, s is the period of vias, and d is the diameter of the vias, as shown in Figure 1. The parameter w_{eff} in this formulation is the most essential design parameter of this SIW six-port junction. Consequently, the cut-off frequency of the TE_{10} mode is obtained from Eq. (2) [6]:

Table 1. S-parameter magnitudes.

Magnitude (dB)	S-parameter
–15	S11
–15	S12
–6	S13
–6	S14
–6	S15
–6	S16
–15	S22
–6	S23
–6	S24
–6	S25
–6	S26

$$f_{c_{10}} = \frac{1}{2w_{eff}\sqrt{\mu\varepsilon}}, \tag{2}$$

where ε is the permittivity and μ the permeability of the dielectric substrate.

2. Analysis and design

The block diagram of the proposed six-port junction is shown in Figure 2. It consists of three 90° hybrid couplers and a T-junction power divider. A simulation is performed by using full wave analysis software on a Rogers 5880 substrate with a thickness of 0.787 mm.

Table 2. Out-port phase differences.

Phase (degrees)	Out-port phase differences
90	Phase (S13) – Phase (S14)
90	Phase (S15) – Phase (S16)
90	Phase (S23) – Phase (S24)
90	Phase (S25) – Phase (S26)

The design goals of S-parameter amplitudes and out-port phase differences are listed in Tables 1 and 2. The initial application of this junction is in QPSK demodulators; however, it also can be used as a reflectometer. Several matching via techniques are applied in order to improve the scattering parameters such as return losses, coupling coefficients, and phase differences.

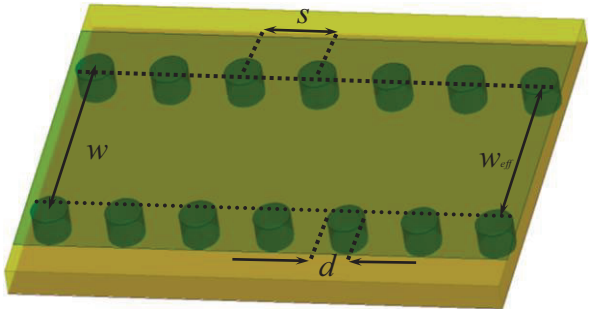

Figure 1. SIW transmission line.

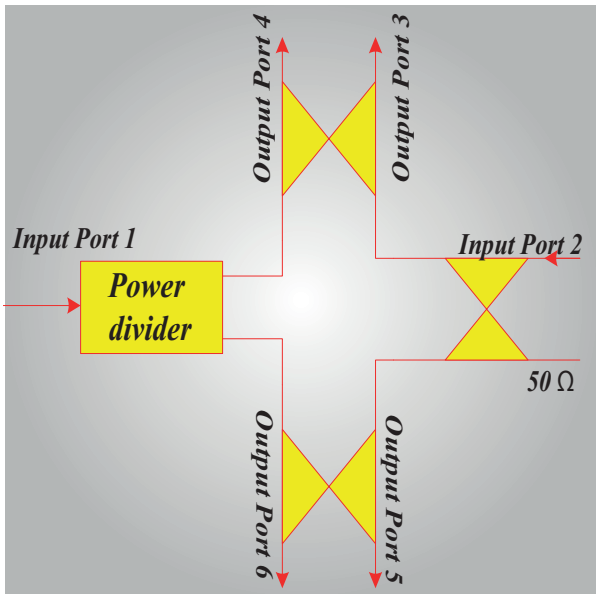

Figure 2. Block diagram of the proposed six-port junction.

2.1. Power divider

The designed power divider in T-form is shown in Figure 3. Without matching vias, this junction will have high return loss due to the reflection of the inputs. The two adjacent vias at the input port have capacitive effects and create symmetric resonance with minimum return loss. The diameters and positions of these vias greatly affect the splitter's input return loss. These posts act as two parallel diaphragms that compensate for the discontinuity (capacitive) effects of the bends, thus improving the coupling between the input and output ports as well as its input return loss.

Table 3. Dimensions of tapered microstrip transition.

	Port 1	Other ports
W_50Ω	2.6 mm	2.6 mm
L_TAPER	5.85 mm	5.85 mm
W_AP	5 mm	3.7 mm

Furthermore, the other inductive vias are forming a parallel inductive diaphragm to creep the waves to outputs. From Eqs. (1) and (2), w is obtained equal to 6.7 mm for output ports at a cut-off frequency of 15.5 GHz. Because of the operating frequency of the junction, this cut-off frequency is an appropriate choice due to a relatively wide frequency range between TE_{10} and TE_{20} modes. The design parameters of this power divider are as follows: $s=$ 0.6 mm, $S1$ = 3.3 mm, $S2$ = 3.2 mm, $S3$ = 0.725 mm, $S4$ = 2.3 mm, $S5$ = 0.4 mm, $d=$0.3 mm, and $D=$0.4 mm. Figure 4 shows simulation results in which the return loss is less than –15 dB and the coupling coefficients are equal to –3 dB in a wide bandwidth with respect to the center frequency of 22.25 GHz.

2.2. The 90° hybrid coupler

There are three 90° hybrid couplers in this design, which play an essential role in the overall performance of the structure. The designed 90° hybrid coupler is shown in Figure 5. The array of via holes is acting as a boundary

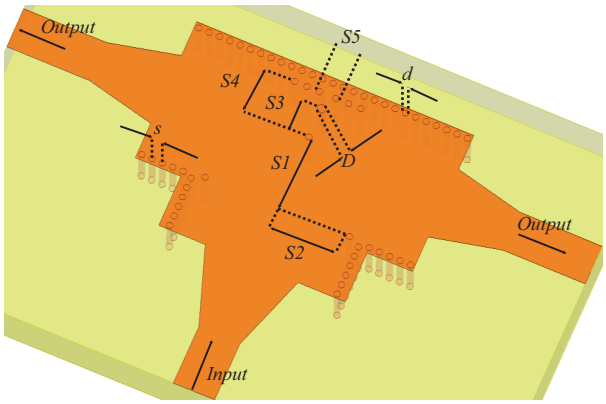

Figure 3. Schematic of the considered power divider.

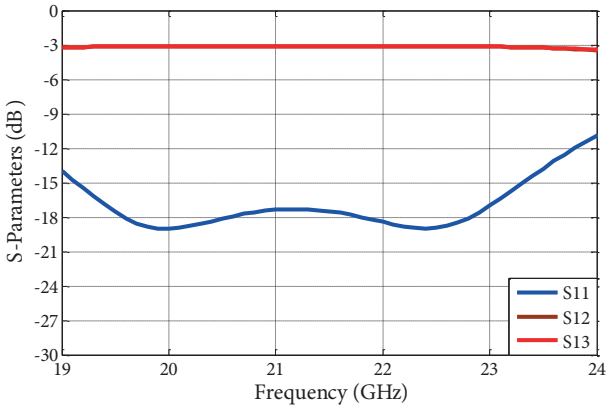

Figure 4. Simulation results of SIW power divider.

to guide the EM waves to the outputs. This compact design has the special advantage of coupling adjustment by changing the length of aperture L1 between two middle rows of the via and can be easily integrated with other components to shape the entire six-port junction. L1 is optimized to gain the best coupling and reflection coefficients. The simulation results of the amplitude of scattering parameters are shown in Figure 6.

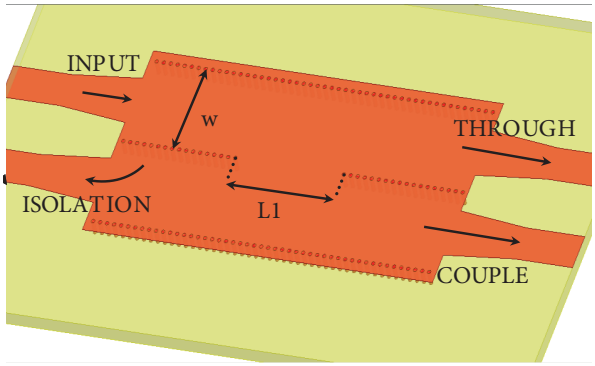

Figure 5. The 90° hybrid coupler in SIW form.

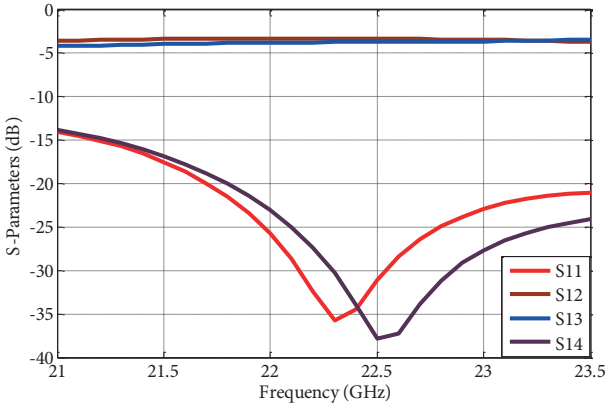

Figure 6. Simulation results of S-parameter magnitudes.

The phase difference of the couple and through ports, as shown in Figure 7, is equal to 90°. The design goals are approximately realized at the entire bandwidth of 21–23.5 GHz.

2.3. Six-port design

Figure 8 shows the mechanical configuration of the proposed structure, in which the building SIW blocks, including three 90° hybrid couplers and a power divider, are merged to form the compact SIW six-port junction. One of the advantages of this design model is that no phase shifter has been utilized, which leads to a wider overall bandwidth. The seventh port is matched to a 50-Ω standard load. This structure is designed and optimized using FEM full wave simulation on a Rogers 5880 substrate with a relative dielectric constant of 2.2, dielectric loss tangent of 0.0009, and thickness of 0.787 mm.

A tapered transition is designed for connecting SMA connectors. The tapered microstrip transition has many advantages, including its full coverage of SIW bandwidth and its better performance compared to other transitions [7,8]. Its structure creates a good matching between the electromagnetic field in the microstrip and

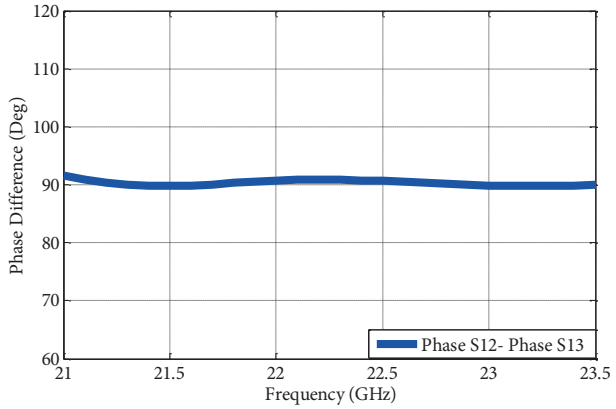

Figure 7. Simulation results of out-port phase differences.

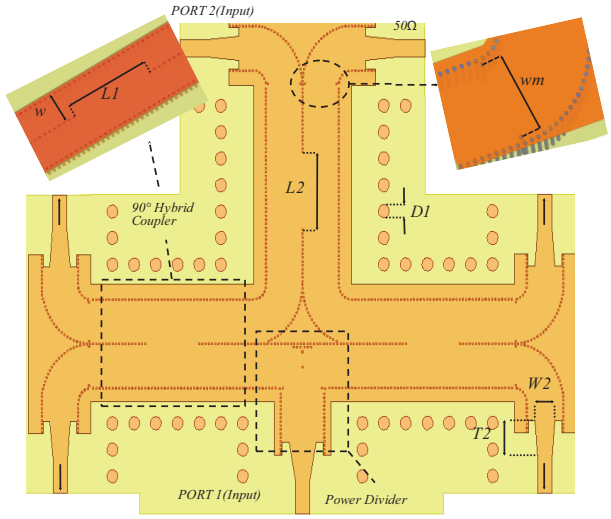

Figure 8. Mechanical configuration of proposed six-port junction.

the SIW that leads to lower losses [9]. This transition matches a 50-Ω microstrip transmission line to SIW, as shown in Figure 9. Its dimensions are listed in Table 3.

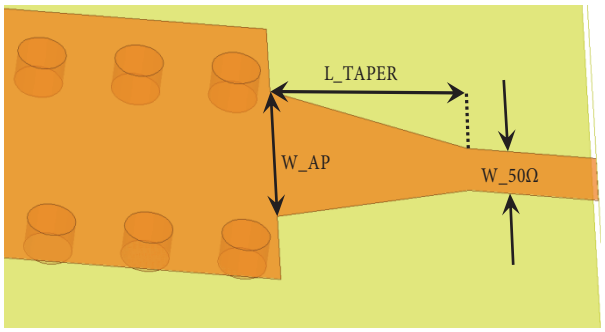

Figure 9. Tapered transition from microstrip to SIW.

The remaining design parameters in Figure 8 have the following dimensions: L1 = 9.9 mm, L2 = 11.7 mm, w = 6.7 mm, wp = 8 mm, wm = 5.9 mm, D1 = 1 mm. The two capacitive vias, with a distance of wm at the ports of the hybrid couplers, are placed to improve impedance matching as well as coupling coefficients.

3. Experimental results

Figure 10 shows the simulation and measurement results of return loss and isolation S-parameter magnitudes due to input ports. It can be observed that the return loss and isolation coefficients are lower than –15 dB across the entire bandwidth. The experimental results of the input return losses are lower than –20 dB at the center frequency of 22.25 GHz. Additionally, Figures 11–14 show the simulation and measurement results of coupling parameters between the input and output ports. It is found that the simulated and measured results are well matched, and the transmission coefficients are close to the theoretical predicted value of –6 dB over the operating frequency range. It should be noted that the initial simulation results obtained with the finite element method (FEM) are verified with the finite difference time domain (FTDT) method before the fabrication process. Figures 15 and 16 show the simulation and measurement results of phase differences

between the output ports. The 90° phase difference between individual coupling S-parameters is of primary importance here.

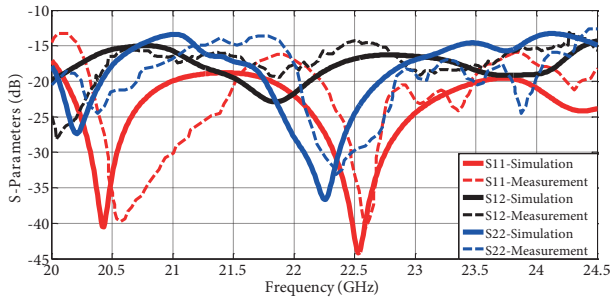

Figure 10. Simulation and measurement results of return-loss and isolation S-parameter magnitudes.

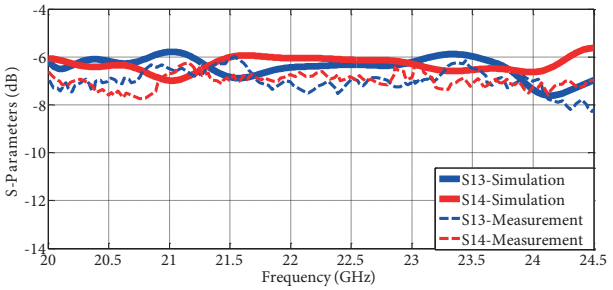

Figure 11. Simulation and measurement results of S-parameter magnitudes, ports 1, 3, and 4.

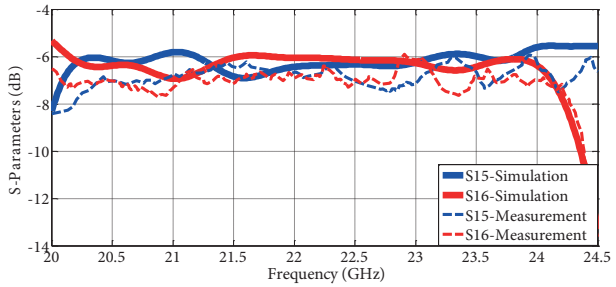

Figure 12. Simulation and measurement results of S-parameter magnitudes, ports 1, 5, and 6.

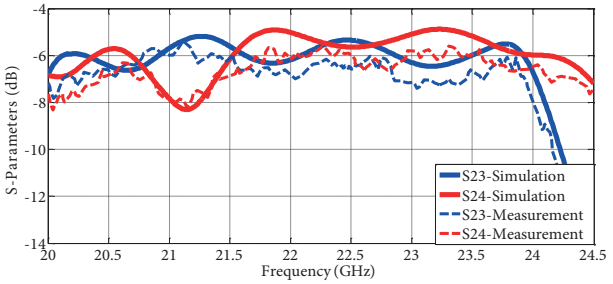

Figure 13. Simulation and measurement results of S-parameter magnitudes, ports 2, 3, and 4.

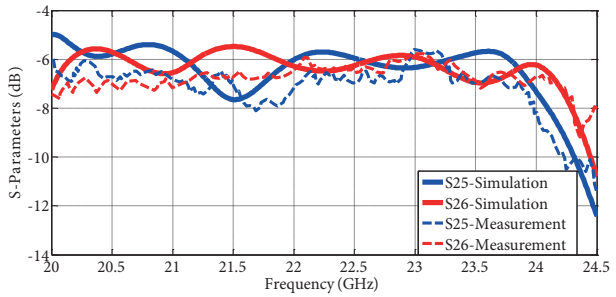

Figure 14. Simulation and measurement results of S-parameter magnitudes, ports 2, 5, and 6.

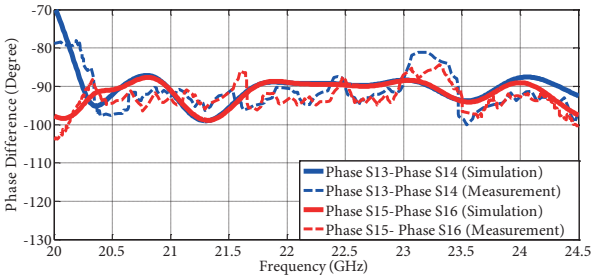

Figure 15. Simulation and measurement results of phase differences between port 1 and output ports S-parameters.

4. Discussion

It can be concluded from Figures 10–16 that all the design goals of this six-port junction have been approximately realized. The inevitable differences are due to fabrication limits such as SMA losses and nonideal cylindrical vias. Several capacitive and inductive vias were inserted to improve the S-parameters of the six-port junction. Significant reduction in insertion loss is obtained because of the changes in the capacitive and inductive effects introduced, due to central vias at the input of the power divider. Referring to Figures 10–16, the design goals of the junction are achieved over almost the entire bandwidth with a center frequency of 22.25 GHz. Figure 17 shows the prototype of this six-port junction.

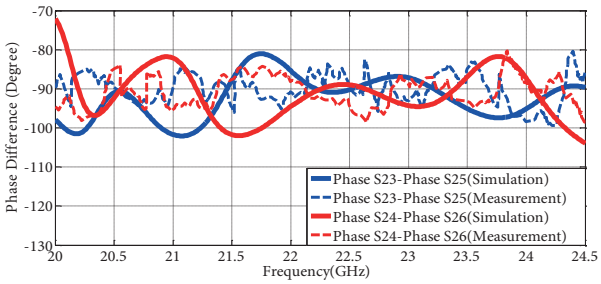

Figure 16. Simulation and measurement results of phase differences between port 2 and output ports S-parameters.

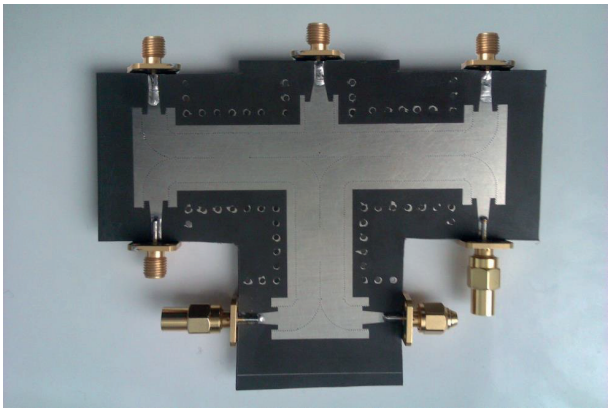

Figure 17. Prototype of the proposed six-port junction.

5. Conclusion

A sub-K-band SIW six-port junction was designed and tested. The measurement results of the magnitude of the coupling parameters agree with the simulation results or are even better in some single frequencies over the operating bandwidth. Furthermore, the return losses are lower than –20 dB at the center frequency of 22.25 GHz. The required 90° phase differences have been realized between the input and output ports. The proposed fabricated prototype can be used in reliable high-power broadband applications at millimeter waves because of its waveguide nature, e.g., as the main heart of an SDR or reflectometer.

References

[1] Deslandes D, Wu K. Accurate modeling, wave mechanisms, and design considerations of a substrate integrated waveguide. IEEE T Microw Theory 2006; 54: 2516-2526.

[2] Perregrini L, Arcioni P, Bressan M, Wu K, Conciauro G, Cassivi Y. Dispersion characteristics of substrate integrated rectangular waveguide. IEEE Microw Wirel Comp 2002; 12: 333-335.

[3] Xu F, Wu K. Guided-wave and leakage characteristics of substrate integrated waveguide. IEEE T Microw Theory 2005; 53: 66-73.

[4] Yan L, Hong W, Wu K, Cui TJ. Investigations on the propagation characteristics of the substrate integrated waveguide based on the method of lines. IEE Proc-H 2005; 152: 35-42.

[5] Chen DP, Wu K. Substrate integrated waveguide filter: basic design rules and fundamental structure features. IEEE Microw Mag 2014; 15: 108-116.

[6] Pozar DM. Microwave Engineering. 4th ed. Hoboken, NJ, USA: Wiley, 2012.

[7] Yang TH, Chen CF, Huang TY, Wang CL, Wu RB. A 60 GHz LTCC transition between microstrip line and substrate integrated waveguide. Proc APMC 2005; I: 4-7.

[8] Deslandes D, Wu K. Analysis and design of current probe transition from grounded coplanar to substrate integrated rectangular waveguides. IEEE T Microw Theory 2005; 53: 2487-2494.

[9] Deslandes D, Wu K. Integrated microstrip and rectangular waveguide in planar form. IEEE Microw Wirel Comp 2001; 11: 68-70.